Lipschitz Stability Estimate for An Initial Wave Reconstruction Problem of Telegraph Type with Gaussian Noise

Dat-Thuc Nguyen, Ngoc Tuan Duong and Vo Anh Khoa

***Abstract*—This work is devoted to the study of an initial wave reconstruction problem of telegraph type. Our specific goal is to determine the initial spikes of an idealized signal in a telegraph wire from two consecutive observations contaminated by Gaussian noise. Our main result shows that the initial reconstruction is Lipschitz stable in the expectation operator. The proof relies upon the integral representation of solution for Cauchy data, together with the use of the truncated Fourier approximator. Additionally, we prove that the reconstructed initial data are exactly observable. Some numerical tests are given to validate our theoretical findings.**

***Index Terms*—Initial wave reconstruction, Telegraph equation, Stability, Exact observability, Gaussian noise.**

I. Introduction

Nowadays, time-dependent coefficient inverse problems are of interest in various applications. These include computed tomography in acoustical problems [1]–[4], reconstructing blood perfusion rates in thermal-wave models [5], recovering the so-called potential in structural geology [6], [7], and several publications cited therein. In this work, we are interested in an inverse model of the telegraph equation with the aim of determining the initial spikes of an idealized signal, which is referred to as the initial wave reconstruction problem of telegraph type.

The telegraph equation is a partial differential equation (PDE) that describes the propagation of electrical signals along transmission lines, helping in understanding various phenomena in telecommunications and signal processing, such as signal distortion, transmission delay, and attenuation. In principle, this equation can be understood as an extension of the more familiar wave equation (cf. [8]), incorporating both wave-like and diffusion-like behavior. Formally, the telegraph equation is expressed as:

$$u_{tt} + (a+b)\, u_t + abu = c^2 u_{xx}, \tag{1}$$

Dat-Thuc Nguyen, Department of Mathematics, Florida State University, Tallahassee, FL 32306, USA, e-mail: tdn23@fsu.edu, ndth1808.hcmus@gmail.com.

Ngoc Tuan Duong, FAMU-FSU College of Engineering, Florida State University, Tallahassee, FL 32310, USA, e-mail: ntd20a@fsu.edu; Department of Electrical and Computer Engineering, North Carolina State University, Raleigh, NC 27695, USA.

Vo Anh Khoa, Department of Mathematics and Statistics, Texas Tech University, Lubbock, TX 79409, USA; Department of Mathematics, Florida A&M University, Tallahassee, FL 32307, USA, e-mail: anhkhoa.vo@ttu.edu, vakhoa.hcmus@gmail.com.

for $(x,t) \in \Omega_T := (0,\ell) \times (0,T)$ and

$$a = \frac{R}{L}, \quad b = \frac{G}{C}, \quad c = \frac{1}{\sqrt{LC}}.$$

Here, u represents the voltage along the transmission line, and L, C, R denote the inductance, capacitance, and resistance per unit length of the transmission line, respectively.

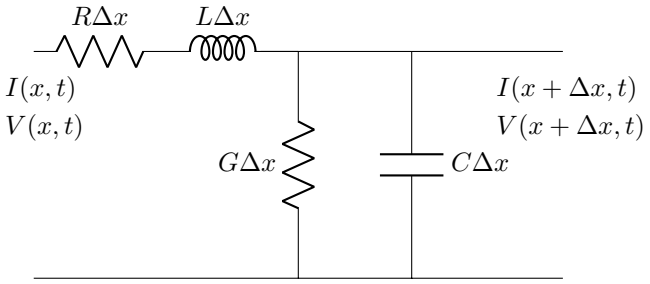

Fig. 1. A typical modeling of a transmission line of a length Δx. In this figure, $V(x,t)$ indicates the voltage at the position x with respect to ground at any time t, and $I(x,t)$ is the current at x and time t. $C(x,t)$ and $G(x,t)$ represent capacitance and conductance to ground; $L(x,t)$ and $R(x,t)$ stand for inductance and resistance, respectively, at x and time t. These result in the total capacitance, conductance, inductance, and resistance $\Delta x C(x,t)$, $\Delta x G(x,t)$, $\Delta x L(x,t)$, $\Delta x R(x,t)$, respectively, for the line of length Δx.

It is worth mentioning that significant efforts have been made in the literature to advance the development of the forward model of the telegraph equation. For instance, Koksal et al. [9] and Mittal et al. [10], [11] have had various numerical studies on different types of the telegraph equation. Recently, Koksal et al. [12] expanded on their contributions by exploring different numerical methods for solving telegraph equations with variable coefficients. Additionally, Cohen and Loughlin [13] developed phase space approximators to analyze the telegraph PDE.

A. Reconstruction model

We assume that the voltage clamped at both ends can be described using the following time-dependent C^2 functions

$$u(0,t) = A(t), \quad u(\ell,t) = B(t) \quad \text{for } t \in (0,T). \tag{2}$$

The reference voltage is $r(x,t) = A(t) + \frac{x}{\ell}[B(t) - A(t)]$. Then, define $v(x,t) = u(x,t) - r(x,t)$. Based on (1), function $v = v(x,t)$ obeys the following PDE:

$$v_{tt} + (a+b)\, v_t + abv = c^2 v_{xx} + F(x,t) \tag{3}$$

for $(x,t) \in \Omega_T$, where

$$F(x,t) = \left(\frac{x}{\ell} - 1\right)\left[A_{tt}(t) + (a+b)\,A_t(t) + abA(t)\right] - \frac{x}{\ell}\left[B_{tt}(t) + (a+b)B_t(t) + abB(t)\right].$$

In this scenario, the non-homogeneous equation (3) satisfies the zero Dirichlet boundary conditions. Now, we state the inverse model of interest.

Initial Wave Reconstruction (IWR). Determine the initial signal $u(x,0) = g_0(x)$ from two consecutive snaphots:

$$u(x,T) = g_T(x), \quad u\left(x,\tilde{T}\right) = h_T(x), \tag{4}$$

where $\tilde{T} = T + \Delta t$ with $\Delta t < 1$ being fixed.

In practice, data measurements always contain noise. Here, to denote noisy functions, we use the superscript ε, which is typically understood as the noise level.

Remark 1. In our theory below, we rely on the terminal data $u_t(x,T) \in L^2(0,\ell)$, and for ease of presentation, we denote $u_t(x,T) = q_T(x)$. By the Taylor expansion of $u\left(x,\tilde{T}\right)$ about $t = T$, we can find a small quantity $\eta_{\Delta t} \in \left(T,\tilde{T}\right)$ such that

$$q_T(x) = \frac{h_T(x) - g_T(x)}{\Delta t} - \frac{\Delta t}{2} u_{tt}(x,\eta_{\Delta t}). \tag{5}$$

Let g_T^ε and h_T^ε be the noisy functions of g_T and h_T, respectively. Accordingly, we define the corresponding terminal data q_T^ε as

$$q_T^\varepsilon(x) = u_t^\varepsilon(x,T) = \frac{h_T^\varepsilon(x) - g_T^\varepsilon(x)}{\Delta t}.$$

In this scenario, we obtain the error estimate between $q_T(x)$, as established in the sense of the Taylor expansion above, and its noisy function $q_T^\varepsilon(x) \in L^2(0,\ell)$, as follows:

$$\|q_T^\varepsilon - q_T\|_{L^2(0,\ell)} \le \frac{2\varepsilon}{\Delta t} + \frac{\Delta t}{2}\|u_{tt}(\eta_{\Delta t})\|_{L^2(0,\ell)},$$

provided that $u_{tt}(\cdot,t) \in L^2(0,\ell)$ for $t \in (T,\tilde{T})$. Note that to get $u_{tt} \in C(T,\tilde{T};L^2(0,\ell))$, we take into account the source condition $u \in C^1(T,\tilde{T};L^2(0,\ell)) \cap C(T,\tilde{T};H^2(0,\ell))$; cf. (1).

B. Outline of the paper

Of particular interest to us is the stability of the IWR when both g_T and h_T are contaminated by Gaussian noise. All definitions related to this stochastic noise can be found in [14], [15], and for clarity, we recall them in section II. From there, we elaborate on the relation between q_T^ε and q_T in this stochastic setting.

Our primary finding is centered around Theorem 6 in section III, leading to the Lipschitz-like stability. To achieve this, we delve into the expansion of the solution by eigen-elements under the assumption that the continuous data q_T is known. Thereby, we also obtain Theorem 5 for the exact observability result. Finally, we present in section IV numerical results to corroborate our theoretical findings, followed by some conclusions and future work to summarize the paper in section V.

II. Gaussian noise for the snapshots

Gaussian process is a stochastic process or a collection of random variables, such that every finite collection of those random variables has a multivariate normal distribution. The distribution of a Gaussian process is the joint distribution of all those random variables, and as such, it is a distribution over functions with a continuous domain.

Definition II.1. A time continuous stochastic process or a sequence of random variables $\{X_t : t \in T\}$ in a probability space is Gaussian process if and only if for every finite set of indices $t_1,\dots,t_k$ in the index set T

$$\mathbf{X}_{t_1,\dots,t_k} = (X_{t_1},\dots,X_{t_k})$$

is a multivariate Gaussian random variable.

In the following, $\mathcal{H}$ is a Hilbert space.

Definition II.2. The stochastic error is a Hilbert-space process or a bounded linear operator $\xi : \mathcal{H} \to L^2(\Omega,\mathcal{A},P)$ where $(\Omega,\mathcal{A},P)$ is a complete probability space and $L^2(\cdot)$ is the space of all square integrable measurable functions.

Thus, for every g_1 and $g_2 \in \mathcal{H}$, $\xi(g_1)$ and $\xi(g_2)$ are random variables in $L^2(\Omega,\mathcal{A},P)$ by defining $\mathbf{E}[\xi(g_1)] = 0, \mathbf{E}[\xi(g_2)] = 0$. Then, we define their covariance Cov_ξ as the bounded linear operator ($\|\mathrm{Cov}_\xi\| \le 1$) from $\mathcal{H}$ to $\mathcal{H}$ such that $\langle \mathrm{Cov}_\xi g_1, g_2\rangle = \mathrm{Cov}(\xi(g_1),\xi(g_2))$.

Definition II.3. The operator ξ is a Gaussian white noise process in $\mathcal{H}$, if $\mathrm{Cov}_\xi = I$ and the induced random variables are Gaussian, this means for all functions $g_1, g_2 \in \mathcal{H}$

$$\xi(g_1),\xi(g_2) \sim \mathcal{N}(0,\|g_1\|^2), \mathcal{N}(0,\|g_2\|^2),$$

and $\mathrm{Cov}(\xi(g_1),\xi(g_2)) = \langle g_1, g_2\rangle$.

Lemma 2. *Let ξ be a Gaussian white noise in $\mathcal{H}$ and $\{\psi_j\}_{j\in\mathbb{N}}$ be an orthonormal basis in $\mathcal{H}$. Then, $\{\xi(\psi_j)\}_{j\in\mathbb{N}}$ are i.i.d. standard Gaussian random variables.*

Proof. One can find the proof of this lemma in [14]. □

From now on, we suppose to observe our two consecutive snapshots (cf. (4)) in the presence of Gaussian white noise processes ξ_1, ξ_2, i.e.

$$g_T^\varepsilon(x) = g_T(x) + \varepsilon\xi_1(x), \quad h_T^\varepsilon(x) = h_T(x) + \varepsilon\xi_2(x), \tag{6}$$

Thereby, the relation between the boundary data q_T and its noisy one q_T^ε is given by

$$q_T^\varepsilon(x) = q_T(x) + \frac{\varepsilon[\xi_2(x) - \xi_1(x)]}{\Delta t} + \frac{\Delta t}{2} u_{tt}(x,\eta_{\Delta t}). \tag{7}$$

Accordingly, assuming that the observations (6) can only be obtained in a discretized form, we only have two vectors of normally distributed random variables $\left\{u_T^{\varepsilon,j}\right\}_{j=\overline{1,m}}, \left\{u_{\tilde{T}}^{\varepsilon,j}\right\}_{j=\overline{1,m}}$ and a vector $\left\{q_T^j\right\}_{j=\overline{1,m}}$ given by

$$g_T^{\varepsilon,j} := \langle u_T^\varepsilon, \psi_j\rangle = \langle g_T, \psi_j\rangle + \varepsilon\xi_1(\psi_j), \tag{8}$$

$$h_T^{\varepsilon,j} := \langle u_{\tilde{T}}^\varepsilon, \psi_j\rangle = \langle h_T, \psi_j\rangle + \varepsilon\xi_2(\psi_j), \tag{9}$$

$$q_T^{\varepsilon,j} := \langle q_T^\varepsilon, \psi_j\rangle = \langle q_T, \psi_j\rangle + \frac{\varepsilon[\xi_2(\psi_j) - \xi_1(\psi_j)]}{\Delta t} + \frac{\Delta t}{2}\langle u_{tt}(\eta_{\Delta t}), \psi_j\rangle, \tag{10}$$

where $m \in \mathbb{N}$ is the number of discrete observations. Note that in our numerical results below, we impose the uniform constraint on ξ_1, ξ_2 in (10), $|\xi_2(\psi_j) - \xi_1(\psi_j)| < \Delta t$, to ensure the same scale of smallness in all types of data being used.

Besides, $\{\psi_n\}_{n\in\mathbb{N}}$ is an orthonormal basis of $L^2(0,\ell)$ and $\psi_n \in H_0^1(0,\ell) \cap C[0,\ell]$ for all $n \in \mathbb{N}$. We also recall the Dirichlet eigenvalues $\{\lambda_n\}_{n\in\mathbb{N}}$ forming an infinite sequence which goes to infinity, viz.

$$0 \le \lambda_0 < \lambda_1 < \lambda_2 < \dots, \text{ and } \lim_{n\to\infty} \lambda_n = \infty.$$

In this one-dimensional setting, we remark that

$$\lambda_n = \left(\frac{n\pi}{\ell}\right)^2, \quad \psi_n(x) = \sqrt{\frac{2}{\ell}} \sin\left(\frac{n\pi}{\ell} x\right). \tag{11}$$

Note that our observations are not in general elements of $L^2(0,\ell)$. Henceforth, assuming the true ones are smooth enough such that $g_T, h_T \in H^{2p}(0,\ell)$ for $p > 0$, we employ the so-called truncated Fourier approximators and rely on them to prove the target stability result. In principle, we make use of the following lemma.

Lemma 3. *Let $g \in H^{2p}(0,\ell)$ for $p > 0$ and $g^\varepsilon(x) = g(x) + \varepsilon\xi(x)$, where ξ is a Gaussian white noise. Let $G^{\varepsilon,m} \in L^2(0,\ell)$ be the truncated Fourier approximator of g^ε,*

$$G^{\varepsilon,m} = \sum_{j=1}^{m} \langle g^\varepsilon, \psi_j\rangle \psi_j,$$

where $m \in \mathbb{N}$ is the number of steps of discrete observations. Then, the following estimate holds

$$\boldsymbol{E}\left(\|G^{\varepsilon,m} - g\|^2_{L^2(0,\ell)}\right) \le \varepsilon^2 m + \frac{\|g\|^2_{H^{2p}(0,\ell)}}{\lambda_m^{2p}}.$$

Proof. Cf. [16], the proof of this lemma is very straightforward. Indeed, we see that

$$\begin{aligned}
&\mathbf{E}\left(\|G^{\varepsilon,m} - g\|^2_{L^2(0,\ell)}\right) \\
&= \mathbf{E}\left(\sum_{j=1}^{m} \langle g^\varepsilon - g, \psi_j\rangle^2\right) + \sum_{j=m+1}^{\infty} \langle g, \psi_j\rangle^2 \\
&= \varepsilon^2 \mathbf{E}\left(\sum_{j=1}^{m} \xi(\psi_j)^2\right) + \sum_{j=m+1}^{\infty} \lambda_j^{-2p}\lambda_j^{2p} \langle g, \psi_j\rangle^2.
\end{aligned}$$

As $\xi(\psi_j)$ has standard Gaussian distribution, the target estimation is obtained. □

Remark 4. In terms of $\left\{q_T^{\varepsilon,j}\right\}_{j=\overline{1,m}}$, consider $Q_T^{\varepsilon,m}$ as its truncated Fourier approximator. Then, proceeding as in Lemma 3, we obtain

$$\begin{aligned}
\mathbf{E}\left(\|Q_T^{\varepsilon,m} - q_T\|^2_{L^2(0,\ell)}\right) &\le \frac{6m\varepsilon^2}{\Delta t^2} \\
&+ \frac{3\Delta t^2}{4}\|u_{tt}(\eta_{\Delta t})\|^2_{L^2(0,\ell)} + \frac{\|q_T\|^2_{H^{2p}(0,\ell)}}{\lambda_m^{2p}}.
\end{aligned}$$

Cf. (1) and (5), to fulfill $q_T \in H^{2p}(0,\ell)$, one can take into account the source condition $u \in C^1(0,\tilde{T}; H^{2p}(0,\ell)) \cap C(0,\tilde{T}; H^{2p+2}(0,\ell))$.

III. Main results

This section is two-fold. First, we employ the method of eigenfunction expansion to derive the integral representation of v, provided that the continuous data q_T is known. In this scenario, we also prove the exact observability of the initial data for the telegraph equation. Second, we prove the Lipschitz stability (with respect to ε) for the IWR problem. This is our target of this paper. Our proof relies upon the explicit representation of function v in the first part, together with Lemma 3.

A. Integral representation of solution

Observe that $\partial_{xx}\psi_n = -\lambda_n\psi_n$ holds true. Multiplying (3) by the eigenfunction ψ_n and then integrating the resulting equation with respect to x, we arrive at

$$\begin{aligned}
&\partial_{tt}\langle v, \psi_n\rangle + (a+b)\,\partial_t\langle v, \psi_n\rangle \\
&\qquad + \left(ab + \lambda_n c^2\right)\langle v, \psi_n\rangle = \langle F(\cdot,t), \psi_n\rangle.
\end{aligned}$$

By setting $v_n = \langle v, \psi_n\rangle$ and $F_n = \langle F(\cdot,t), \psi_n\rangle$, we solve the non-homogeneous differential equation $v_n'' + (a+b)v_n' + \left(ab + \lambda_n c^2\right)v_n = F_n$. Then, by superposition principle, we take $v_n = w_{1,n} + w_{2,n}$ in which $w_{1,n}$ is the complementary solution and $w_{2,n}$ is known as the particular solution. Letting $g_n = \langle g, \psi_n\rangle$, $q_n = \langle q, \psi_n\rangle$, where two functions g, q are

$$g(x) = g_T(x) - A(T) - [B(T) - A(T)]\frac{x}{\ell}, \tag{12}$$

$$q(x) = q_T(x) - A'(T) - [B'(T) - A'(T)]\frac{x}{\ell}, \tag{13}$$

the complementary solution $w_{1,n}$ satisfies

$$\begin{cases} w_{1,n}'' + (a+b)w_{1,n}' + \left(ab + \lambda_n c^2\right)w_{1,n} = 0, \\ w_{1,n}(T) = g_n, w_{1,n}'(T) = q_n. \end{cases}$$

As to the particular solution, it is of the form $w_{2,n}(t) = z_{1,n}(t)\,y_{1,n}(t) + z_{2,n}(t)\,y_{2,n}(t)$ and satisfies $w_{2,n}(T) = w_{2,n}'(T) = 0$. Here, $y_{1,n}, y_{2,n}$, which will be clarified later, are obtained from the complementary solution $w_{1,n} = C_1(n)\,y_{1,n}(t) + C_2(n)\,y_{2,n}(t)$, and $z_{1,n}, z_{2,n}$ are unknown. By Wronskian rule, we know that

$$z_{1,n}' = \frac{-y_{2,n}F_n}{y_{1,n}y_{2,n}' - y_{2,n}y_{1,n}'}, z_{2,n}' = \frac{y_{1,n}F_n}{y_{1,n}y_{2,n}' - y_{2,n}y_{1,n}'}.$$

For each n, the characteristic equation in this case is $\kappa^2 + (a+b)\kappa + ab + \lambda_n c^2 = 0$, whose roots are $\kappa_n^{\pm} = -d \pm \omega_n$. Here, $d = \frac{a+b}{2}$ and $\omega_n = \frac{1}{2}\sqrt{(a-b)^2 - 4\lambda_n c^2}$. Consider the following sets

$$S_1 := \left\{n \in \mathbb{N} : (a-b)^2 - 4\lambda_n c^2 \ge 0\right\}, \tag{14}$$

$$S_2 := \left\{n \in \mathbb{N} : (a-b)^2 - 4\lambda_n c^2 < 0\right\}. \tag{15}$$

Low-frequency mode: If $n \in S_1$, ω_n is real and thus, $w_{n,1}(t) = C_1(n)\,y_{1,n}(t) + C_2(n)\,y_{2,n}(t)$, where $y_{1,n}(t) =$

$e^{\kappa_n^+ t}$ and $y_{2,n}(t) = e^{\kappa_n^- t}$. This gives $y_{1,n}y'_{2,n} - y_{2,n}y'_{1,n} = (\kappa_n^- - \kappa_n^+)\, e^{\kappa_n^+ t} e^{\kappa_n^- t}$ and

$$z_{1,n}(T) - z_{1,n}(t) = -\frac{1}{\kappa_n^- - \kappa_n^+}\int_t^T e^{-\kappa_n^+ s} F_n(s)\, ds,$$
$$z_{1,n}(T) - z_{2,n}(t) = \frac{1}{\kappa_n^- - \kappa_n^+}\int_t^T e^{-\kappa_n^- s} F_n(s)\, ds.$$

It is clear that $z_{1,n}(T), z_{2,n}(T)$ must satisfy the following system so these functions are such that $w'_{2,n}(T) = 0$.

$$\begin{cases} z_{1,n}(T)e^{\kappa_n^+ T} + z_{1,n}(T)e^{\kappa_n^- T} = 0 \\ z_{1,n}(T)\kappa_n^+ e^{\kappa_n^+ T} + z_{1,n}(T)\kappa_n^- e^{\kappa_n^- T} = 0 \end{cases}$$

By this way, the particular solution $w_{2,n}$ is obtained.

Now, evaluating $w_{1,n}$ and its derivative $w'_{1,n}$ at $t = T$ yields

$$\begin{cases} C_1(n)\,\kappa_n^+ e^{\kappa_n^+ T} + C_2(n)\,\kappa_n^- e^{\kappa_n^- T} = q_n, \\ C_1(n)\, e^{\kappa_n^+ T} + C_2(n)\, e^{\kappa_n^- T} = g_n. \end{cases}$$

Solving this system leads to

$$w_{1,n}(t) = \frac{q_n - \kappa_n^- g_n}{\kappa_n^+ - \kappa_n^-} e^{\kappa_n^+ (t-T)} + \frac{\kappa_n^+ g_n - q_n}{\kappa_n^+ - \kappa_n^-} e^{\kappa_n^- (t-T)}.$$

Hence, the sought solution $v_n = w_{1,n} + w_{2,n}$ is obtained, viz.

$$\begin{aligned} v_n(t) = e^{d(T-t)} &\left[\frac{-(q_n + dg_n)\sinh(\omega_n(T-t))}{\omega_n} \right. \\ &\left. + g_n \cosh(\omega_n(T-t)) \right] \\ &- \int_t^T \frac{e^{d(s-t)} \sinh(\omega_n(t-s))\, F_n(s)}{\omega_n} ds. \end{aligned} \tag{16}$$

High-frequency mode: If $n \in S_2$, ω_n is purely imaginary number, then we take its imaginary part. Therefore, $w_{1,n}(t) = e^{-dt}[C_1(n)\cos(\omega_n t) + C_2(n)\sin(\omega_n t)]$. This means that $y_{1,n}(t) = e^{-dt}\cos(\omega_n t)$ and $y_{2,n}(t) = e^{-dt}\sin(\omega_n t)$, leading to $y_{1,n}y'_{2,n} - y_{2,n}y'_{1,n} = e^{-2dt}\omega_n$. Thus, we find that

$$z_{1,n}(T) - z_{1,n}(t) = -\int_t^T \frac{e^{ds}\sin(\omega_n s)\, F_n(s)}{\omega_n} ds,$$
$$z_{2,n}(T) - z_{2,n}(t) = \int_t^T \frac{e^{ds}\cos(\omega_n s)\, F_n(s)}{\omega_n} ds.$$

It is easy to check that $z_{1,n}(T) = z_{2,n}(T) = 0$ and $w'_{2,n}(T) = 0$. Thereby, the particular solution $w_{2,n}$ is obtained. Now, evaluating $w_{1,n}$ and $w'_{1,n}$ at $t = T$ yields

$$\begin{cases} \frac{q_n + dg_n}{\omega_n} e^{dT} = -C_1(n)\sin(\omega_n T) + C_2(n)\cos(\omega_n T), \\ g_n e^{dT} = C_1(n)\cos(\omega_n T) + C_2(n)\sin(\omega_n T). \end{cases}$$

This system admits the following $C_1(n)$ and $C_2(n)$

$$C_1 = e^{dT}\left[\frac{-(q_n + dg_n)\sin(\omega_n T)}{\omega_n} + g_n\cos(\omega_n T)\right],$$
$$C_2 = e^{dT}\left[\frac{(q_n + dg_n)\cos(\omega_n T)}{\omega_n} + g_n\sin(\omega_n T)\right].$$

Therefore, we can conclude the complementary solution $w_{1,n}(t)$. Hence, the sought solution $v_n = w_{1,n} + w_{2,n}$ is also concluded, viz.

$$\begin{aligned} v_n(t) = e^{d(T-t)} &\left[\frac{-(q_n + dg_n)\sin(\omega_n(T-t))}{\omega_n} \right. \\ &\left. + g_n \cos(\omega_n(T-t)) \right] \\ &- \int_t^T \frac{e^{d(s-t)} \sin(\omega_n(t-s))\, F_n(s)}{\omega_n} ds. \end{aligned} \tag{17}$$

Overall, our solution to the telegraph equation (1) can be written in the following form

$$u(x,t) = \sum_{n \in S_1 \cup S_2} v_n(t)\psi_n(x) + r(x,t). \tag{18}$$

Now we are in a position to study the exact observability result before deriving the stability estimate. The idea behind observability is the property that knowledge of the output data over a finite interval uniquely determines the initial state.

Let the space of initial conditions be $Z = H^1(0,\ell) \times L^2(0,\ell)$. We accordingly define an observability map from $Z \to Z$ as

$$\mathcal{L}^T \begin{bmatrix} v(x,0) \\ v_t(x,0) \end{bmatrix} = \begin{bmatrix} v(x,T) \\ v_t(x,T) \end{bmatrix}. \tag{19}$$

Cf. [8], for equation (1) with the zero Dirichlet boundary conditions, the system is said to be exactly observable under $\mathcal{L}^T$ on $[0,T]$ if the initial state can be uniquely and continuously constructed from knowledge of the output in $L^2(0,T;Z)$.

At this stage, it is vital to find out the form of the derivative of u with respect to t. In the sequel, we define two functions

$$S_n(t',t) = \begin{cases} \sinh(\omega_n(t'-t)) & \text{for } n \in S_1, \\ \sin(\omega_n(t'-t)) & \text{for } n \in S_2, \end{cases} \tag{20}$$

$$C_n(t',t) = \begin{cases} \cosh(\omega_n(t'-t)) & \text{for } n \in S_1, \\ \cos(\omega_n(t'-t)) & \text{for } n \in S_2. \end{cases} \tag{21}$$

Observe that u_t can be written in the form

$$u_t(x,t) = \sum_{n \in S_1 \cup S_2} v'_n(t)\psi_n(x) + r_t(x,t), \tag{22}$$

where

$$\begin{aligned} v'_n(t) = &\\ e^{d(T-t)} &\left[q_n C_n(T,t) + \left(\frac{dq_n + d^2 g_n}{\omega_n} \mp \omega_n g_n \right) S_n(T,t) \right] \\ + \int_t^T &e^{d(s-t)} \left[\frac{d}{\omega_n} S_n(t,s) - C_n(t,s) \right] F_n(s) ds. \end{aligned} \tag{23}$$

Remark in (23) and below that by the $\mp$ we mean, the "$-$" is valid when $n \in S_1$, and the "$+$" is enabled when $n \in S_2$. Now, we state the theorem for the exact observability result.

Theorem 5. *System (1)-(2) with Cauchy observations at $t = T$, $u(x,T) \in H^1(0,\ell)$ and $u_t(x,T) \in L^2(0,\ell)$, is exactly observable under the mapping $\mathcal{L}^T$.*

Proof. The proof of this theorem is presented in the Appendix. □

B. Stability estimate

Now we prove the Lipschitz stability estimate for the IWR problem. By the presence of m, the number of discrete observations, in the data, we denote by $u^{\varepsilon,m}$ the solution of the IWR problem. Based upon the integral representation of v, cf. (12) and (13), we consider two functions $g^\varepsilon, q^\varepsilon$:

$$g^\varepsilon(x) = g_T^\varepsilon(x) - A(T) - [B(T) - A(T)]\,\frac{x}{\ell}, \tag{24}$$

$$q^\varepsilon(x) = q_T^\varepsilon(x) - A'(T) - [B'(T) - A'(T)]\,\frac{x}{\ell}, \tag{25}$$

Accordingly, the truncated Fourier approximators of these functions are given by

$$G^{\varepsilon,m}(x) = \sum_{j=1}^{m} g^{\varepsilon,j}\psi_j(x), \quad Q^{\varepsilon,m}(x) = \sum_{j=1}^{m} q^{\varepsilon,j}\psi_j(x),$$

Similar to (22), $u^{\varepsilon,m}$ has the following form:

$$u^{\varepsilon,m}(x,t) = \sum_{n\in\mathbb{N}} v_n^{\varepsilon,m}(t)\psi_n(x) + r(x,t), \tag{26}$$

where q_n and g_n in $v_n^{\varepsilon,m}(t)$ are, respectively, replaced by

$$Q_n^{\varepsilon,m} = \langle Q^{\varepsilon,m}, \psi_n\rangle, G_n^{\varepsilon,m} = \langle G^{\varepsilon,m}, \psi_n\rangle.$$

Theorem 6. *Let u be the true solution of problem (1)-(2) associated with the true data $g_T, q_T \in H^{2p}(0,\ell)$ for $p > 0$. Let $u^{\varepsilon,m}$ be the solution of problem (1)-(2) subject to the Gaussian noisy data $g_T^\varepsilon, q_T^\varepsilon$ with m discrete observations. Then, the following estimate holds*

$$\begin{aligned}
&\boldsymbol{E}\left(\|u^{\varepsilon,m}(\cdot,t) - u(\cdot,t)\|^2_{L^2(0,\ell)}\right)\\
&\le 3e^{2d(T-t)}\left[\left(M_{C,n_0}^2 + \frac{d^2}{\omega_{n_0}^2}M_{S,n_0}^2\right)\left(\varepsilon^2 m + \frac{\|g\|^2_{H^{2p}(0,\ell)}}{\lambda_m^{2p}}\right) + \frac{M_{S,n_0}^2}{\omega_{n_0}^2}\left(\frac{6m\varepsilon^2}{\Delta t^2} + \frac{3\Delta t^2}{4}\|u_{tt}(\eta_{\Delta t})\|^2_{L^2(0,\ell)} + \frac{\|q\|^2_{H^{2p}(0,\ell)}}{\lambda_m^{2p}}\right)\right],
\end{aligned}$$

where $M_{S,n_0}, M_{C,n_0} > 0$ are independent of Δt and ε, m, and $\omega_{n_0}^2 = \frac{1}{4}\left|(a-b)^2 - 4\lambda_{n_0}c^2\right|$ for a finite $n_0 \in \mathbb{N}$.

Proof. By (22), (26) and using direct calculations, we estimate that

$$\begin{aligned}
\|u^{\varepsilon,m}(\cdot,t) - u(\cdot,t)\|^2_{L^2(0,\ell)} &= e^{2d(T-t)}\left\|\sum_{n\in\mathbb{N}}\left((G_n^{\varepsilon,m} - g_n)\left(C_n(T,t) - \frac{d}{\omega_n}S_n(T,t)\right) - \frac{(Q_n^{\varepsilon,m} - q_n)}{\omega_n}S_n(T,t)\right)\psi_n\right\|^2_{L^2(0,\ell)}\\
&\le 3e^{2d(T-t)}\left(\frac{1}{2}\left\|\sum_{n\in\mathbb{N}}(G_n^{\varepsilon,m} - g_n)\left(C_n(T,t) - \frac{d}{\omega_n}S_n(T,t)\right)\psi_n\right\|^2_{L^2(0,\ell)} + \left\|\sum_{n\in\mathbb{N}}\frac{(Q_n^{\varepsilon,m} - q_n)}{\omega_n}S_n(T,t)\psi_n\right\|^2_{L^2(0,\ell)}\right),
\end{aligned}$$

where we have used Minkowski's inequality and the elementary inequality $(a+b)^2 \le 3(\frac{a^2}{2} + b^2)$.

Observe that S_1 is of a non-zero finite measure. Particularly, in this set, $|\omega_n| = \frac{1}{2}\sqrt{(a-b)^2 - 4\lambda_n c^2}$ decreases as n increases. Meanwhile, in S_2, $|\omega_n| = \frac{1}{2}\sqrt{4\lambda_n c^2 - (a-b)^2}$ increases to the infinity. Therefore, there exists a finite number $n_0 \in \mathbb{N}$ such that $|\omega_n|$ is minimized. Accordingly, the minimal value of $|\omega_n|$ is denoted by $|\omega_{n_0}|$. Cf. (20) and (21), the existence of such a n_0 guarantees that we can find the upper bounds M_{S,n_0} and M_{C,n_0} of $S_n(T,t)$ and $C_n(T,t)$ over $[0,T]$ for all $n \in \mathbb{N}$.
Thus, by Parseval's identity, we have

$$\begin{aligned}
\left\|\sum_{n\in\mathbb{N}}(G_n^{\varepsilon,m} - g_n)\left(C_n(T,t) - \frac{d}{\omega_n}S_n(T,t)\right)\psi_n\right\|^2_{L^2(0,\ell)} &= \sum_{n\in\mathbb{N}}|\langle G^{\varepsilon,m} - g, \psi_n\rangle|^2\left(C_n(T,t) - \frac{d}{\omega_n}S_n(T,t)\right)^2\\
&\le 2\left(M_{C,n_0}^2 + \frac{d^2}{\omega_{n_0}^2}M_{S,n_0}^2\right)\left(\sum_{n\le m}|\langle g^\varepsilon - g, \psi_n\rangle|^2 + \sum_{n>m}|\langle g, \psi_n\rangle|^2\right).
\end{aligned}$$

Using Lemma 3, one obtains the following estimate in the expectation manner,

$$\mathbf{E}\left(\left\|\sum_{n\in\mathbb{N}}(G_n^{\varepsilon,m} - g_n)\left(C_n(T,t) - \frac{d}{\omega_n}S_n(T,t)\right)\psi_n\right\|^2_{L^2(0,\ell)}\right) \le 2\left(M_{C,n_0}^2 + \frac{d^2}{\omega_{n_0}^2}M_{S,n_0}^2\right)\left(\varepsilon^2 m + \frac{\|g\|^2_{H^{2p}(0,\ell)}}{\lambda_m^{2p}}\right) \tag{27}$$

By the same process, we also get the estimate for the second sum

$$\mathbf{E}\left(\left\|\sum_{n\in\mathbb{N}}\frac{(Q_n^{\varepsilon,m} - q_n)}{\omega_n}S_n(T,t)\psi_n\right\|^2_{L^2(0,\ell)}\right) \le \frac{M_{S,n_0}^2}{\omega_{n_0}^2}\left(\frac{6m\varepsilon^2}{\Delta t^2} + \frac{3\Delta t^2}{4}\|u_{tt}(\eta_{\Delta t})\|^2_{L^2(0,\ell)} + \frac{\|q\|^2_{H^{2p}(0,\ell)}}{\lambda_m^{2p}}\right) \tag{28}$$

Combining (27), (28), we complete the proof of the theorem. □

The Lipschitz stability estimate is a direct consequence of the central Theorem 6. Indeed, let $\hat{u}^{\varepsilon,m}$ be the solution to the same system with two consecutive snapshots $\hat{g}_T, \hat{h}_T$. Then, proceeding as in the proof of Theorem 6, we obtain the following estimate:

$$\mathbf{E}\left(\|u^{\varepsilon,m}(\cdot,t)-\hat{u}^{\varepsilon,m}(\cdot,t)\|^2_{L^2(0,\ell)}\right) \le 3e^{2d(T-t)}\left[\left(M^2_{C,n_0}+\frac{d^2}{\omega^2_{n_0}}M^2_{S,n_0}\right)\|g^\varepsilon-\hat{g}^\varepsilon\|^2_{L^2(0,\ell)}+\frac{M^2_{S,n_0}}{\omega^2_{n_0}}\|q^\varepsilon-\hat{q}^\varepsilon\|^2_{L^2(0,\ell)}\right]. \tag{29}$$

Furthermore, if we choose $m=\lfloor\varepsilon^{-\alpha}\rfloor$, the greatest integer less than or equal to $\varepsilon^{-\alpha}$, and $\Delta t=\varepsilon^\beta$, for all $\alpha\in(0,2)$ and $\beta>0$, then the following Hölder rates of convergence hold true

$$\begin{aligned}\mathbf{E}\left(\|u^{\varepsilon,m}(\cdot,t)-u(\cdot,t)\|^2_{L^2(0,\ell)}\right) \le 3e^{2d(T-t)}&\left[\left(M^2_{C,n_0}+\frac{d^2}{\omega^2_{n_0}}M^2_{S,n_0}\right)\left(\varepsilon^{2-\alpha}+\frac{\varepsilon^{4\alpha p}\|g\|^2_{H^{2p}(0,\ell)}\ell^{4p}}{(1-\varepsilon^\alpha)^{4p}\pi^{4p}}\right)\right.\\&\left.+\frac{M^2_{S,n_0}}{\omega^2_{n_0}}\left(6\varepsilon^{2-\alpha+2\beta}+\frac{3\varepsilon^{2\beta}}{4}\|u_{tt}(\eta_{\Delta t})\|^2_{L^2(0,\ell)}+\frac{\varepsilon^{4\alpha p}\|q\|^2_{H^{2p}(0,\ell)}\ell^{4p}}{(1-\varepsilon^\alpha)^{4p}\pi^{4p}}\right)\right].\end{aligned}$$

IV. Numerical results

A. Forward solver and numerical settings

In our numerical settings, a uniform grid of mesh points $(x,t)=(x_h,t_k)$ are used. Here $x_h=(h-1)\Delta x$ and $t_k=(k-1)\Delta t$ for $1\le h\le N_x$ and $1\le k\le N_t$ where $\Delta x=\frac{\ell}{N_x-1}, \Delta t=\frac{T}{N_t-1}$ and $N_x, N_t\in\mathbb{N}$. Herewith, we choose $N_x=600$ and $N_t=600$. We need such a high value of N_x to get a good resolution for our graphical illustration (since the cable is long, 10 km). Meanwhile, as we use the Riemann sum for time integration, taking $N_t=600$ helps to ensure the accuracy of the entire reconstruction process. Last but not least, such a choice of N_x and N_t satisfy the stability condition of the forward model; see (31).

Here, we expound upon our forward solver for the data generation of the inverse model. Our forward solver means solving (1) with (2) and the initial data $u(x,0)=g_0(x)$, $u_t(x,0)=0$. We have chosen the initial time derivative to be zero for simplicity.

The forward solver can be derived using the same method of eigenfunction expansion. However, to avoid the so-called inverse crime (cf. e.g. [17], [18]), we deliberately apply the conventional finite difference method. For clarity, the fully discrete version of Equation (1) is given by

$$\frac{u_h^{k+1}-2u_h^k+u_h^{k-1}}{(\Delta t)^2}+(a+b)\frac{u_h^{k+1}-u_h^{k-1}}{2\Delta t}+abu_h^k = c^2\frac{u_{h+1}^k-2u_h^k+u_{h-1}^k}{(\Delta x)^2}. \tag{30}$$

Let $A_1=\frac{a+b}{2}\Delta t, A_2=ab(\Delta t)^2$ and $A_3=c^2\left(\Delta t/\Delta x\right)^2$. Cf. [19], the stability of the scheme (30) is guaranteed if $0<A_3<1-\frac{A_2}{4}$, or equivalently,

$$N_t>\sqrt{c^2(N_x-1)^2\left(\frac{T}{\ell}\right)^2+\frac{abT^2}{4}}+1. \tag{31}$$

In our numerical results below, we do not choose the true solution of (1). Instead, we choose its boundary data at two ends $A(t), B(t)$ and the initial function g_0. Then, the data for g_T and h_T are obtained from the forward solution at $t=T$ and $t=T+\Delta T$. Accordingly, q_T is approximated by a first-order divided difference. Besides, $\Delta T=0.01$ is fixed.

As for our choices of A, B and g_0, we, cf. [20], take into account the following compatibility conditions:

$$\begin{cases}A(0)=g_0(0), B(0)=g_0(\ell), A'(0)=B'(0)=0,\\ A''(0)+abg_0(0)=c^2g_0''(0),\\ B''(0)+abg_0(\ell)=c^2g_0''(\ell).\end{cases} \tag{32}$$

Based on [21], we take parameter data for 24-gauge telephone polyethylene insulated cable (PIC) at 70°F with $R=172.28\ \Omega$/km, $L=612.5\ \mu$H/km, $G=0.072\ \mu$S/km and $C=51.57$ nF/km. The length of the underlying cable is $\ell=10$ km, and the observation time is $T=10$ s. Thereby, all the coefficients in (1) are calculated as

$$a=0.2813, b=0.0014, c=0.0056, d=0.1413.$$

As seen, we mainly utilize inner products to demonstrate the solutions. To calculate them numerically, we apply the standard Filon quadrature method; cf. e.g. [22]. For the time integral in v_n, we use the standard Riemann sum.

As readily expected, we need truncation to compute the infinite sum of the inverse solution; see (26). The truncation number, called N, is chosen such that the following relative error is fulfilled:

$$E(N,g_0)=\frac{\left\|g_0-\sum_{n=1}^N\langle g_0,\psi_n\rangle\psi_n\right\|_{L^2}}{\|g_0\|_{L^2}}<1\%. \tag{33}$$

As to the data reliability, we define that the data is reliable if the relative error between g_0 and the reconstructed initial spikes from our inverse problem with noiseless data is less than 1% and N satisfies (33).

Remark 7. There are numerous numerical differentiation techniques developed to compute the contaminated Neumann data q_T^ε; see e.g. [23] and references cited therein. However, it is beyond the scope of our inceptive work to apply other techniques. Cf. Remark 1, the most natural finite difference approach being used provides us with the direct estimation between the exact and noisy Neumann data, leading to our central convergence theorem.

B. Test 1: Modulated wave with $A(t) = B(t) = 0$

In this test, we choose

$$g_0(x) = \exp\left(-\frac{x}{10}\right)\sin\left(\frac{3\pi x}{10}\right)\sin(4\pi x).$$

We remark that this case satisfies 4 out of 6 compatibility conditions in (32), while the last two are approximately fulfilled, i.e. $A''(0) + abg_0(0) = B''(0) + abg_0(\ell) = 0$ and $c^2 g_0''(0) \approx 0.0037$, $c^2 g_0''(\ell) \approx -0.0013$.

By increasing N, we see the relative error E decreases gradually. Notably, we get $E(63, g_0) = 1.0476\%$ and $E(64, g_0) = 0.9354\%$, indicating that we need at least $N = 64$ to meet condition (33). Besides, we note that the relative error between g_0 and the (noiseless) reconstructed spikes is 0.9988%; see in the first column of Figure 2 the graphical illustration of the spikes compared with the true one. This ensures the data reliability for our inverse model.

We report that the relative error between the noisy reconstructed signal $u^{\varepsilon,m}$ ($m = 100$) at $t = 0$ and the true one g_0 decreases significantly from 179.7513% (for $\varepsilon = 10^{-1}$) to 17.5534% (for $\varepsilon = 10^{-3}$) and 1.0180% (for $\varepsilon = 10^{-5}$). As can be seen in the first column of Figure 4, when ε reduces to 10^{-3}, the reconstruction becomes great in shape. Similar observation can be found in the data; see the first row of Figure 3. We also remark that even though the measurement of Dirichlet data at $t = T$ performs well in shape when $\varepsilon = 10^{-1}$, the performance of the corresponding Neumann data is in a different situation. This is the main factor that hinders us from getting a good initial reconstruction.

C. Test 2: Square-like wave with $A(t) = t^3 e^{-t^2}$, $B(t) = 0$

In this test, we take

$$g_0(x) = \sum_{n=1}^{5} \frac{\sin\left[(2n-1)\pi x\right]}{2n-1}.$$

Here, the square-like signal g_0 and A, B satisfy all compatibility conditions (32). Numerically, we find that $N = 45$ is the optimal choice for the truncation number since $E(44, g_0) = 10.2118\%$ and $E(45, g_0) = 0.0058\%$. On the other hand, the relative error between g_0 and the noiseless reconstructed spikes is 0.1101%, which shows the data reliability of our forward solver. Graphs of these functions are presented in the second column of Figure 2.

Similar to what we have observed in Test 1, the reconstruction becomes good when $\varepsilon = 10^{-3}$; see the second column of Figure 4. In particular, when decreasing ε from 10^{-1} to 10^{-3}, the relative error between the noisy reconstructed signal and the true one reduces more than 100 times from 605.9129% to 5.8719%. And when $\varepsilon = 10^{-5}$, this error goes under 1%, particularly 0.1333%. This essentially shows a good accuracy of the reconstruction process. We also depict in the second row of Figure 3 the performance of the Cauchy observations for different values of $\varepsilon \in \{10^{-1}, 10^{-3}, 10^{-5}\}$.

D. Test 3: Sawtooth-like wave with $A(t) = B(t) = t^3 e^{-t^2}$

In this last test, we consider

$$g_0(x) = \sum_{n=1}^{5} \frac{\sin(n\pi x)}{n}.$$

Note that by the choices of g_0 and A, B, all compatibility conditions (32) are fulfilled.

To check the data reliability, we see from the forward solver that the relative error E stays under 1% (cf. (33) for the criteria) once $N = 50$. In particular, we have $E(50, g_0) = 0.0014\%$ compared to $E(49, g_0) = 16.5316\%$. Moreover, we report that the relative error between g_0 and the noiseless reconstructed spikes yields 0.1931%, as also consistently visualized in the last column of Figure 2.

As to the noisy reconstruction, we find it similar to the previous tests, albeit the complication in the shape of the true initial data. When $\varepsilon = 10^{-1}$, the relative error between the noisy reconstruction and the true one is huge, 539.7934%. This is due to the entire loss of accuracy in the Neumann data, while the Dirichlet measurement shows the acceptable shape; see the last row of Figure 3. Once $\varepsilon = 10^{-3}$, the relative error then reduces significantly to 5.8310%. We also report that this error drops under 1% (0.1845% to be exact) when $\varepsilon = 10^{-5}$. To graphically see the entire accurate reconstruction process, the reader can be referred to the last column of Figure 4.

Remark 8. Taking into account the relative error between the noiseless and noisy reconstructed spikes for all tests, we see the consistency of our Lipschitz stability estimate (29). Approximately, the error is reduced by a factor of 100, corresponding to the reduction in ε. In Test 1, we particularly observe that the error decreases significantly from 180.3735% with $\varepsilon = 10^{-1}$ to 17.5850% with $\varepsilon = 10^{-3}$, and further to 0.1826% with $\varepsilon = 10^{-5}$. Similarly, in Test 2, the error reduces from 606.0757% ($\varepsilon = 10^{-1}$) to 5.8649% ($\varepsilon = 10^{-3}$) and then to 0.0655% ($\varepsilon = 10^{-5}$). In Test 3, we report the error decreasing from 540.0488% with $\varepsilon = 10^{-1}$ to 5.8502% with $\varepsilon = 10^{-3}$, and finally to 0.0579% with $\varepsilon = 10^{-5}$.

V. Conclusions and Future Work

We have studied the initial reconstruction of the telegraph equation from the data at two Gaussian contaminated consecutive snapshots. Using the so-called truncated Fourier approximator, we have obtained the Lipschitz stability estimate of the reconstruction. We have also added to the theoretical findings the exact observability result. Several numerical experiments are conducted to verify the stability of the reconstruction.

By using the method of eigenfunction expansion, our theoretical findings can be similarly obtained for Dirichlet, Neumann, and Robin cases in rectangle-like domains $\Omega = [0, l_1] \times \ldots \times [0, l_d] \subset \mathbb{R}^d$ (with $l_i > 0$); cf. [24]. The extension may also work for circular annuli, spheres, and similar shapes when the eigen-elements are derived explicitly. In principle, as long as the eigen-elements satisfy the theoretical properties of non-negative and increasing-to-infinity eigenvalues, and complete and orthonormal eigenfunctions, the same derivations apply. However, the problem will become more challenging if arbitrarily complicated (Lipschitz) domains are taken into account. In that case, numerical methods for the eigenvalue problem are needed. This discrete framework, together with the perspective of non-constant coefficients, will be our upcoming target.

Our future work will, on the other hand, include the Neumann data reconstruction $u_t(x, 0)$. In that perspective, just like what have been done for the conventional Stefan problem [25],

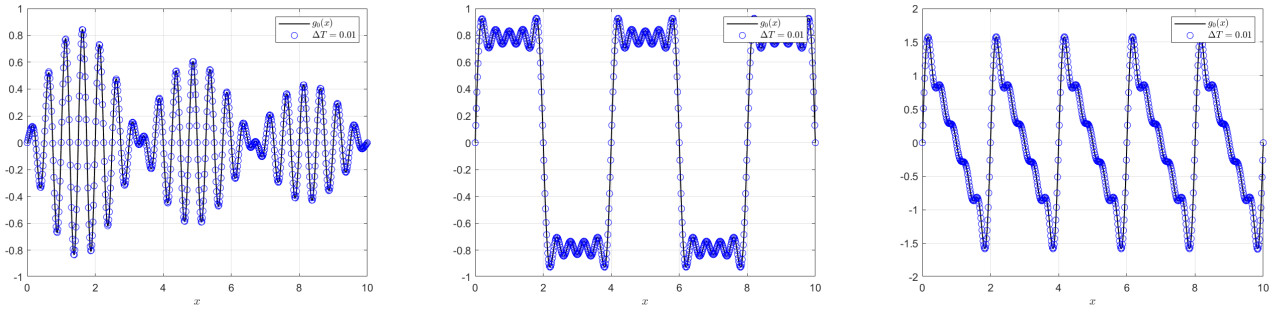

(a) Test 1 (b) Test 2 (c) Test 3

Fig. 2. Reconstructed initial spikes in Tests 1, 2, 3 from noiseless data with $\Delta T = 0.01$. Graphs of the true initial data g_0 are also presented to show the data reliability.

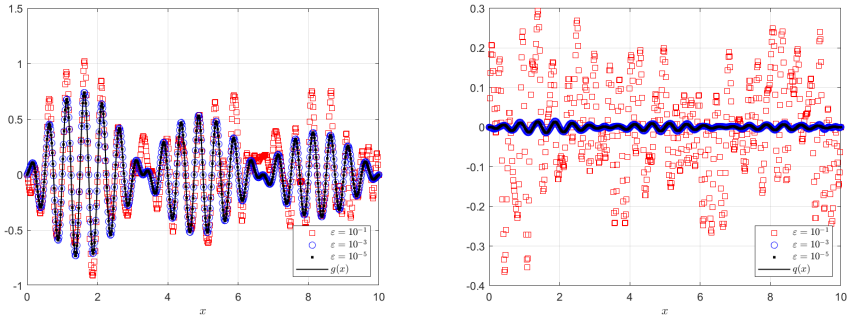

(a) Test 1

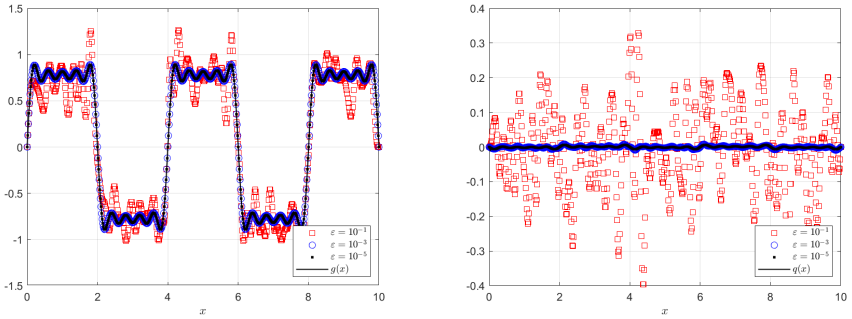

(b) Test 2

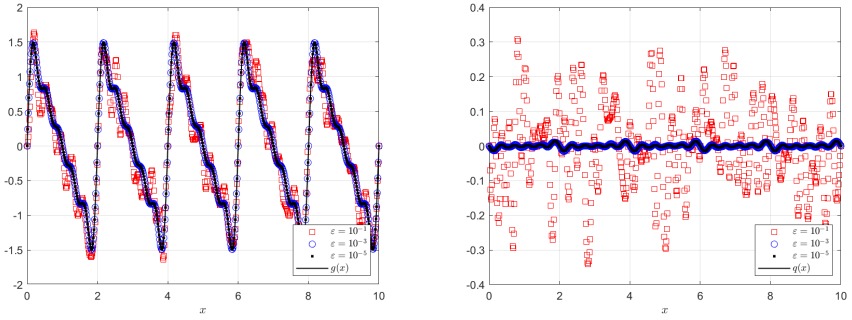

(c) Test 3

Fig. 3. Gaussian contaminated data ($G^{\varepsilon,m}$ and $Q^{\varepsilon,m}$) and true data (g and q) in Tests 1, 2, 3 with 100 samples and $\varepsilon \in \{10^{-1}, 10^{-3}, 10^{-5}\}$.

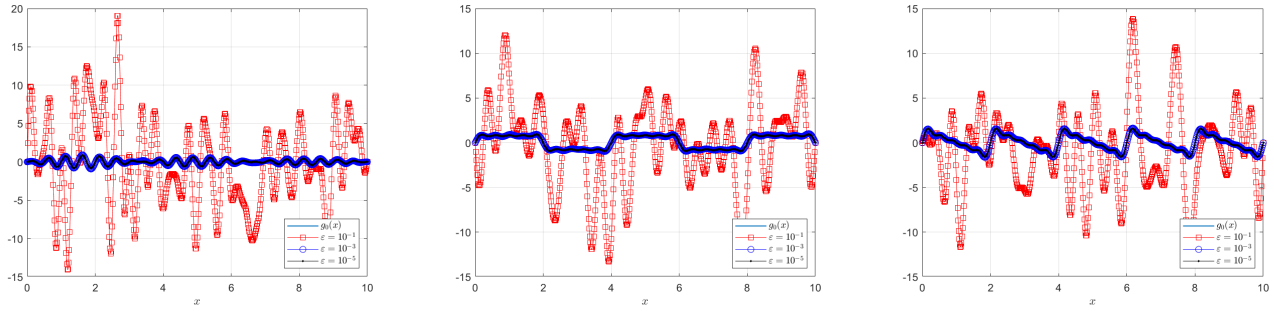

(a) Test 1 (b) Test 2 (c) Test 3

Fig. 4. Numerical comparison between the noisy reconstructed solution and the true solution in Tests 1, 2, 3 with 100 samples and $\varepsilon \in \{10^{-1}, 10^{-3}, 10^{-5}\}$.

some regularization may be needed if a stable result cannot be obtained for the noisy data.

ACKNOWLEGMENT

This work was supported by the National Science Foundation grant #DMS-2316603. D.-T.N. thanks Dr. Mai Hoang Bien (VNU-University of Science) for his guidance and support during D.-T.N.'s studies at VNU-University of Science. N.T.D. would like to extend his sincerest thanks to the supervisors and teachers Drs. Chul Kim, Sastry Pamidi, and Peter Cheetham (Florida State University) for their guidance and support during N.T.D.'s undergraduate years. V.A.K. thanks Dr. Le Minh Triet (Saigon University) and Dr. Boussetila Nadjib (Université 8 mai 1945 - Guelma) for their initial support.

DECLARATIONS

The authors declare no competing interests.

REFERENCES

[1] M. Haltmeier, L. Neumann, and S. Rabanser, "Single-stage reconstruction algorithm for quantitative photoacoustic tomography," *Inverse Problems*, vol. 31, no. 6, p. 065005, may 2015. [Online]. Available: https://dx.doi.org/10.1088/0266-5611/31/6/065005

[2] J. Bae, B. Kwon, and S. Moon, "Reconstruction of the initial state from the data measured on a sphere for plasma-acoustic wave equations," *Inverse Problems*, vol. 34, no. 10, p. 105004, aug 2018. [Online]. Available: https://dx.doi.org/10.1088/1361-6420/aad343

[3] T. T. Le, L. V. Nguyen, L. H. Nguyen, and H. Park, "The time dimensional reduction method to determine the initial conditions without the knowledge of damping coefficients," *Computers & Mathematics with Applications*, vol. 166, pp. 77–90, 2024. [Online]. Available: https://www.sciencedirect.com/science/article/pii/S0898122124001706

[4] T. D. Dang, L. H. Nguyen, and H. T. T. Vu, "Determining initial conditions for nonlinear hyperbolic equations with time dimensional reduction and the Carleman contraction," Dec. 2023.

[5] Y.-L. Fang, D. Lesnic, and M. Alosaimi, "Inverse problems of damped wave equations with Robin boundary conditions: an application to blood perfusion," *Inverse Problems*, vol. 39, no. 6, p. 065008, apr 2023. [Online]. Available: https://dx.doi.org/10.1088/1361-6420/acca42

[6] A. A. Kutsenko, "Recovery of defects from the information at detectors," *Inverse Problems*, vol. 32, no. 5, p. 055005, 2016. [Online]. Available: https://dx.doi.org/10.1088/0266-5611/32/5/055005

[7] S. Chang and V. H. Weston, "On the inverse problem of the 3d telegraph equation," *Inverse Problems*, vol. 13, no. 5, p. 1207, oct 1997. [Online]. Available: https://dx.doi.org/10.1088/0266-5611/13/5/007

[8] J. Tang, J. Liu, and M. Xiao, "Reconstruction of initial wave with radiation boundary condition via boundary sensing," *Wave Motion*, vol. 91, p. 102383, 2019. [Online]. Available: https://doi.org/10.1016/j.wavemoti.2019.102383

[9] M. E. Koksal, M. Senol, and A. K. Unver, "Numerical simulation of power transmission lines," *Chinese Journal of Physics*, vol. 59, pp. 507–524, 2019. [Online]. Available: https://www.sciencedirect.com/science/article/pii/S0577907319300140

[10] R. Mittal and R. Bhatia, "Numerical solution of second order one dimensional hyperbolic telegraph equation by cubic B-spline collocation method," *Applied Mathematics and Computation*, vol. 220, pp. 496–506, 2013. [Online]. Available: https://www.sciencedirect.com/science/article/pii/S0096300313006619

[11] ——, "A numerical study of two dimensional hyperbolic telegraph equation by modified B-spline differential quadrature method," *Applied Mathematics and Computation*, vol. 244, pp. 976–997, 2014. [Online]. Available: https://www.sciencedirect.com/science/article/pii/S0096300314010170

[12] M. E. Koksal, "Recent developments of numerical methods for analyzing telegraph equations," *Archives of Computational Methods in Engineering*, vol. 30, 2023. [Online]. Available: https://link.springer.com/article/10.1007/s11831-023-09909-w#citeas

[13] L. Cohen and P. Loughlin, "Phase space analysis of the telegraph equation," *IEEE Transactions on Antennas and Propagation*, vol. 70, no. 10, pp. 9687–9693, 2022.

[14] L. Cavalier, *Inverse Problems in Statistics*, P. Alquier, E. Gautier, and G. Stoltz, Eds. Berlin, Heidelberg: Springer Berlin Heidelberg, 2011. [Online]. Available: https://doi.org/10.1007/978-3-642-19989-9_1

[15] N. H. Tuan, V. A. Khoa, P. T. K. Van, and V. V. Au, "An improved quasi-reversibility method for a terminal-boundary value multi-species model with white gaussian noise," *Journal of Computational and Applied Mathematics*, vol. 384, p. 113176, 2021. [Online]. Available: https://www.sciencedirect.com/science/article/pii/S0377042720304672

[16] P. N. Duc, E. Nane, O. Nikan, and N. A. Tuan, "Approximation of the initial value for damped nonlinear hyperbolic equations with random Gaussian white noise on the measurements," *AIMS Mathematics*, vol. 7, no. 7, pp. 12 620–12 634, 2022. [Online]. Available: https://www.aimspress.com/article/doi/10.3934/math.2022698

[17] J. L. Mueller and S. Siltanen, *Linear and Nonlinear Inverse Problems with Practical Applications*. Society for Industrial and Applied Mathematics, Oct. 2012.

[18] V. Tahmasbi, S. M. H. Karimian, and S. Noori, "An inverse front tracking method for modeling solidification process in a smelting furnace," *Applied Thermal Engineering*, vol. 248, p. 123300, Jul. 2024.

[19] R. K. Mohanty, "An unconditionally stable difference scheme for the one-space-dimensional linear hyperbolic equation," *Applied Mathematics Letters*, vol. 17, no. 1, pp. 101–105, Jan. 2004.

[20] R. Temam, "Suitable initial conditions," *Journal of Computational Physics*, vol. 218, no. 2, pp. 443–450, 2006. [Online]. Available: https://www.sciencedirect.com/science/article/pii/S0021999106001884

[21] W. D. Reeve, *Subscriber Loop Signaling and Transmission Handbook*. IEEE Press, 1995.

[22] M. Abramowitz and I. A. Stegun, *Handbook of Mathematical Functions: With Formulas, Graphs, and Mathematical Tables*, ser. Applied mathematics series. Dover Publications, 1965. [Online]. Available: https://books.google.com/books?id=V3ZQAAAAMAAJ

[23] P. M. Nguyen, T. T. Le, L. H. Nguyen, and M. V. Klibanov, "Numerical differentiation by the polynomial-exponential basis," *Journal of Applied and Industrial Mathematics*, vol. 17, no. 4, pp. 928–942, 2023.

[24] D. S. Grebenkov and B.-T. Nguyen, "Geometrical structure of Laplacian eigenfunctions," *SIAM Review*, vol. 55, no. 4, pp. 601–667, 2013. [Online]. Available: https://doi.org/10.1137/120880173

[25] G. M. M. Reddy, M. Vynnycky, and J. A. Cuminato, "An efficient adaptive boundary algorithm to reconstruct Neumann boundary data in the MFS for the inverse Stefan problem," *Journal of Computational and Applied Mathematics*, vol. 349, pp. 21–40, 2019.

APPENDIX: PROOF OF THEOREM 5

First, we show that $\mathcal{L}^T$ is injective. To do so, we take into account the forward mapping from $t = 0$ to $t = T$. Below, for simplicity, let $h_0(x) = u(x,0) - r(x,0)$ and $k_0(x) = u_t(x,0) - r_t(x,0)$, and we, respectively, denote the inner product between them and ψ_n by h_n and k_n. Cf. (17) and (19)–(21), we have

$$\mathcal{L}^T \begin{bmatrix} v(x,0) \\ v_t(x,0) \end{bmatrix} = \begin{bmatrix} v(x,T) \\ v_t(x,T) \end{bmatrix} = e^{-dT} \begin{bmatrix} \displaystyle\sum_{n\in\mathbb{N}} \left(h_n C_n(T,0) + \frac{k_n + dh_n}{\omega_n} S_n(T,0) + \int_0^T \frac{e^{ds} S_n(T,s) F_n(s)}{\omega_n} ds \right) \psi_n(x) \\ \displaystyle\sum_{n\in\mathbb{N}} \left\{ k_n C_n(T,0) - \left(\frac{dk_n + d^2 h_n}{\omega_n} \mp \omega_n h_n \right) S_n(T,0) \right. \\ \qquad \left. - \displaystyle\int_0^T e^{ds} \left[\frac{d}{\omega_n} S_n(T,s) - C_n(T,s) \right] F_n(s) ds \right\} \psi_n(x) \end{bmatrix}.$$

To prove the injectivity of $\mathcal{L}^T$, we suppose that $[\tilde{v}(x,T), \tilde{v}_t(x,T)]^T = [v(x,T), v_t(x,T)]^T$ in Z. In addition, the initial data associated with $\tilde{v}$ are $\tilde{h}_0$ and $\tilde{k}_0$, corresponding to h_0 and k_0, respectively. Thus, we accordingly denote the inner product between them ($\tilde{h}_0$ and $\tilde{k}_0$) and ψ_n by $\tilde{h}_n$ and $\tilde{k}_n$. Then, we set $H_n = \tilde{h}_n - h_n$ and $K_n = \tilde{k}_n - k_n$. By the injectivity's definition, we deduce the following system of two equations:

$$\begin{aligned} &K_n \frac{S_n(T,0)}{\omega_n} + H_n \left(C_n(T,0) + \frac{d}{\omega_n} S_n(T,0) \right) = 0, \\ &K_n \left(\frac{1}{d} C_n(T,0) - \frac{1}{\omega_n} S_n(T,0) \right) - H_n \left(\frac{d}{\omega_n} \mp \frac{\omega_n}{d} \right) S_n(T,0) = 0. \end{aligned}$$

By Crammer's rule, we obtain $H_n = 0$ and $K_n = 0$ for all $n \in \mathbb{N}$, which directly implies the injectivity of the operator $\mathcal{L}^T$. Next, let $[v(x,T), v_t(x,T)]^T \in Z$. By the integral representation of v above, we can construct $[v(x,0), v_t(x,0)]^T$. Furthermore, by (16), (17), (23), it indicates that $[v(x,0), v_t(x,0)]^T \in Z$. Henceforth, $\mathcal{L}^T$ is bijective.
The inverse operator of $\mathcal{L}^T$, denoted by $\mathcal{L}^T_{-1}$, is given as

$$\mathcal{L}^T_{-1} \begin{bmatrix} v(x,T) \\ v_t(x,T) \end{bmatrix} = \begin{bmatrix} v(x,0) \\ v_t(x,0) \end{bmatrix} = e^{dT} \begin{bmatrix} \displaystyle\sum_{n\in\mathbb{N}} \left(g_n C_n(T,0) - \frac{q_n + dg_n}{\omega_n} S_n(T,0) - \int_0^T \frac{e^{d(s-T)} S_n(0,s) F_n(s)}{\omega_n} ds \right) \psi_n(x) \\ \displaystyle\sum_{n\in\mathbb{N}} \left\{ q_n C_n(T,0) + \left(\frac{dq_n + d^2 g_n}{\omega_n} \mp \omega_n g_n \right) S_n(T,0) \right. \\ \qquad \left. + \displaystyle\int_0^T e^{d(s-T)} \left[\frac{d}{\omega_n} S_n(0,s) - C_n(0,s) \right] F_n(s) ds \right\} \psi_n(x) \end{bmatrix}.$$

Now, we show that the inverse of $\mathcal{L}^T$ is bounded on its range. Notice that $e^{d(s-T)} \le 1$ for all s in $[0,T]$ and recall from (20) and (21) that there exist two upper bounds M_{C,n_0} and M_{S,n_0} of $C_n(0,s)$ and $S_n(0,s)$ on $[0,T] \times \{0\}$. Moreover, we can find $n_0 \in \mathbb{N}$ such that $|\omega_{n_0}| \le |\omega_n|$ for all $n \in \mathbb{N}$. Therefore, for $v(x,0)$, using Parseval's identity, we estimate that

$$\begin{aligned} \frac{1}{3} \|v(\cdot,0)\|^2_{L^2(0,\ell)} &\le \sum_{n\in\mathbb{N}} g_n^2 \left(M_{C,n_0} + \frac{d}{\omega_n} M_{S,n_0} \right)^2 + \sum_{n\in\mathbb{N}} q_n^2 \frac{M^2_{S,n_0}}{\omega_n^2} + \sum_{n\in\mathbb{N}} \left(\int_0^T \frac{e^{d(s-T)} S_n(s,0) F_n(s)}{\omega_n} ds \right)^2 \\ &\le \left(M_{C,n_0} + \frac{d}{\omega_{n_0}} M_{S,n_0} \right)^2 \|g\|^2_{L^2(0,\ell)} + \frac{M^2_{S,n_0}}{\omega^2_{n_0}} \|q\|^2_{L^2(0,\ell)} + \frac{T M_S^2}{\omega^2_{n_0}} \int_0^T \|F(\cdot,s)\|^2_{L^2(0,\ell)} ds. \end{aligned}$$

By Parseval's identity again, $v_t(x,0)$ is bounded in the sense of L^2 by

$$\begin{aligned} \frac{1}{4} \|v_t(x,0)\|^2_{L^2(0,\ell)} \le &\left(M_{C,n_0} + \frac{d}{\omega_{n_0}} M_{S,n_0} \right)^2 \|q\|^2_{L^2(0,\ell)} + \frac{d^2}{\omega_{n_0}} M^2_{S,n_0} \|g\|^2_{L^2(0,\ell)} + M^2_{S,n_0} \sum_{n\in\mathbb{N}} \omega_n^2 g_n^2 \\ &+ 2T \left(\frac{d^2 M_S^2}{\omega^2_{n_0}} + M^2_{C,n_0} \right) \int_0^T \|F(\cdot,s)\|^2_{L^2(0,\ell)} ds. \end{aligned}$$

As S_1 is finite, we deduce that

$$M_S^2 \sum_{n\in\mathbb{N}} \omega_n^2 g_n^2 = M_S^2 \sum_{n\in S_1} \left[\frac{(a-b)^2}{4} - \lambda_n c^2\right] g_n^2 + M_S^2 \sum_{n\in S_2} \left[\lambda_n c^2 - \frac{(a-b)^2}{4}\right] g_n^2$$
$$\leq M_S^2 \left[\frac{(a-b)^2}{4} \|g\|^2_{L^2(0,\ell)} + c^2 \|g'\|^2_{L^2(0,\ell)}\right].$$

Hence, the inverse of $\mathcal{L}^T$ is bounded on its range, indicating that the system is exactly observable. We complete the proof of the theorem.